Nat. Hazards Earth Syst. Sci. Discuss., 1, 7595–7613, 2013
www.nat-hazards-earth-syst-sci-discuss.net/1/7595/2013/
doi:10.5194/nhessd-1-7595-2013
© Author(s) 2013. CC Attribution 3.0 License.

Natural Hazards and Earth System Sciences
Open Access
Discussions

This discussion paper is/has been under review for the journal Natural Hazards and Earth System Sciences (NHESS). Please refer to the corresponding final paper in NHESS if available.

Numerical simulation of relatively heavy nocturnal rain bands associated with nocturnal coastal fronts in the Mediterranean basin

J. Mazon[1] **and D. Pino**[1,2]

[1]Applied Physics Department, Universitat Politècnica de Catalunya – BarcelonaTech (UPC), Barcelona, Spain
[2]Institute for Space Studies of Catalonia (IEEC–UPC), Barcelona, Spain

Received: 26 November 2013 – Accepted: 3 December 2013 – Published: 18 December 2013

Correspondence to: J. Mazon (jordi.mazon@upc.edu) and D. Pino (david.pino@upc.edu)

Published by Copernicus Publications on behalf of the European Geosciences Union.

Abstract

Three offshore rain bands associated with nocturnal coastal fronts formed near the Israel coastline, the Gulf of Genoa and on the northeastern coast of the Iberian Peninsula are simulated by using version 3.3 of WRF–ARW mesoscale model to study the dynamics of the atmosphere in each case.

A relatively large 1 h and 10 h accumulated precipitation are simulated when comparing with some other similar rain bands formed in the Mediterranean basin. According to the simulations, the coastal fronts formed near the Israel coastline and in the Gulf of Genoa are quasi-stationary, while the one formed on the northeastern of the Iberian Peninsula moves offshore. For the three events, the evolution of the triggering parameter H/LFC, where H is the coastal-front depth and LFC is the Level of Free Convection, is compared and used as an indication of the occurrence of convective precipitation.

1 Introduction

Nocturnal offshore rain bands close to the coastline formed by interaction between drainage wind with a prevailing flow are commonly observed phenomena during the night and early morning in many areas of the world, specially at the tropics. The physical mechanism producing offshore rain bands is well-known. After sunset the inland air cools faster and moves to the coastline along the riverbeds and streams, and the slope of the mountains located close the coast. This cold air mass forms a coastal front when arrives over the sea and interacts with a warmer air mass. As a consequence, the warmer and wetter sea air is lifted over the cold front. When ascending it may condensate and form stratiform clouds if the maritime air reaches the Lifting Condensation Level (LCL). In some cases, convective clouds eventually appear if the Level of Free Convection (LFC) is reached. In any case, the depth of the colder inland air mass (H) plays an important role in helping the wetter and warmer maritime air mass to reach LCL or LFC (Schoenberg, 1984; Miglietta and Rotunno, 2010). These

NHESSD

1, 7595–7613, 2013

last authors conducted idealized numerical studies of the triggering mechanisms which enhance nocturnal convection and they concluded that moderate precipitation occurs if the height of the mountain h is located near or above the LFC. In contrast, stratiform clouds without or weak precipitation are formed if h is approximately equal or higher than but lower than LFC; if h is lower than clear sky prevails. Miglietta and Rotunno (2010) also defined some parameters to explain the intensity and the location of convective rainfall over idealized mountains, as the triggering parameter h/LFC. Values greater than 1 of this parameter suggest that convective cells are appearing over the mountain, while small values indicate that convection is inhibited.

Several authors studied nocturnal fronts at the tropics. Yu and Jou (2004) detected and studied the formation of thunderstorms off the southeast coast of Taiwan. Houze et al. (1981) used radar data to study the effect of the wind cycle and the associated rainfall in Borneo, including nocturnal offshore rain bands. Mori et al. (2004) described the formation of convective systems generated by offshore winds off the coast of Sumatra. Murakami (1983) described during winter months a front caused by drainage winds on the southeast coast of Japan producing an increase in rainfall when compared to other nearby areas. Lau and Yi-Leng (1999) described the nocturnal rainfall in certain regions in Hawaii, attributing it to the formation of a front caused by nocturnal drainage winds. Frye and Chen (2001) studied the evolution of intense drainage winds that generated showers at night also on the island of Hawaii. Ohsawa et al. (2003) analyzed nocturnal precipitation caused by nocturnal fronts over Bangladesh, Thailand, Vietnam and Malaysia. Mapes et al. (2003) described and modeled the rain on the western coast of Panama and Colombia. Wu et al. (2008) studied the nocturnal rainfall offshore in the West Kalimantan Island (Indonesia). Wapler and Lane (2012) studied the nocturnal offshore convection near Darwin (Australia) by using the WRF–ARW mesoscale model (Skamarock et al., 2008).

Despite the large number of references dealing with nocturnal rain bands associated with nocturnal coastal fronts, there is only few studies focusing on nocturnal rain bands in the Mediterranean basin. Probably the most iconic investigation about noctur-

NHESSD
1, 7595–7613, 2013

nal coastal fronts in this basin was made by Neumann (1951). This author proposes convergence between a prevailing synoptic wind and the land breeze to explain the observed offshore convection in southern coast of Israel. In this area, Heiblum et al. (2011) suggest that the concave shape of the coastline has an important role in enhancing the convergence of the land breeze and synoptic winds near the coastline, having a significant effect over the precipitation in the south Israel. Furthermore, Goldreich et al. (2004) describes local nocturnal precipitation from November to September in South Israel produced by a coastal front near the coastline, formed by land breeze interacting with a synoptic flow, having a significant contribution to the total amount of rainfall in this area during the dry years. Mazon and Pino (2013b) simulated by using WRF–ARW mesoscale model several nocturnal coastal fronts at the coasts of Israel, Italia and Libya.

In the western Mediterranean basin, Callado and Pascual (2002) detected nocturnal convection at the mouths of three rivers that flow into the northeastern coast of the Iberian Peninsula. Mazon and Pino (2009) studied the increase of nocturnal precipitation at the mouth of the Llobregat River (close to Barcelona city), which is caused by the interaction between the relatively cold drainage winds and the warm and wet Mediterranean air mass, especially during late summer and early autumn. Mazon and Pino (2013a) simulated by using MM5 mesoscale model (Grell et al., 1994) two events of nocturnal coastal fronts in the south and the northeast of the Iberian Peninsula.

This paper aims to show and describe three events of relatively high intense precipitation associated with nocturnal cold coastal fronts formed near the coast in the Mediterranean basin, caused by the interaction of the drainage cold inland air with a prevailing warmer and wetter air mass, contributing to the knowledge of this phenomenon over the Mediterranean basin. For that purpose, three nocturnal coastal fronts associated with relatively high 1 and 10 h accumulated precipitation with respect to some others studied events in the Mediterranean basin have been selected and simulated by using WRF–ARW mesoscale model. The first selected event (ISR) occurred on the southern coast of Israel on 6 January 2011, and it has been already described

NHESSD
1, 7595–7613, 2013

by Mazon and Pino (2013b). The second event (GEN), occurred in the Gulf of Genoa on 30 January 2008, and the third selected event on the northeastern coast of the Iberian Peninsula (IP) on 6 September 2011. Figure 1 shows the location where these events occurred within the Mediterranean basin. Taking into account that we are not interested in validating the mesoscale model, no comparison between observations and numerical results is made throughout the paper. Several studies have been devoted to investigate this particular subject (Ruiz and Nogues-Paegle, 2010; Jankov et al., 2005; Argueso et al., 2011; Laviola et al., 2011).

The structure of this paper is as follows. Section 2 is devoted to describe the methodology used in this investigation. Section 3 shows the results of the simulations, focused on the analysis of the ISR, GEN and IP events. The paper ends with Sect. 4, where the conclusions are exposed.

2 Methodology

The methodology used to detect and analyze nocturnal rain bands over the Mediterranean basin consists in three steps. First, nocturnal rain bands are detected by using the Tropical Radar Measurement Mission (TRMM) multi-satellite measurements and estimations data (Haddad et al., 1997; Huffman et al., 2007). This multi-satellite is able to record precipitation produced below 37° of latitude. For higher latitudes, the TRMM multi-satellite estimates the precipitation field by using an algorithm (Huffman et al., 2007).

Once an event is detected by TRMM, the second step consists in analyzing the synoptic situation at sea level, 850 hPa and 500 hPa obtained from the NOAA-CR20 and NCEP reanalysis database, in order to discard those events where precipitation is likely caused by other atmospheric mechanisms, as low pressure areas or polar fronts.

Finally, at the third step, the events, where precipitation is not associated with a low pressure system or to polar fronts, but it is more likely due to a coastal front, are simulated by using version 3.3 of the Advanced Research WRF–ARW mesoscale model.

NHESSD
1, 7595–7613, 2013

The WRF–ARW vertical configuration for all the studied events has 42 σ-vertical levels. The number of nested domains used as well as other relevant information about the domains is shown in Table 1. The same physical schemes are used for all the numerical simulations performed. The MRF scheme is used for the PBL parameterization (Hong and Pan, 1996); the RRTM scheme for long wave radiation (Mlawer et al., 1997); the MM5 shortwave scheme for shortwave radiation (Dudhia, 1989) and the WSM scheme for the microphysics parameterization (Hong et al., 2004). No cumulus parameterization is used for the smallest domains because the horizontal resolution is lower than 3 km. The initial and boundary conditions were updated every 6 h with information obtained from the ECMWF reanalysis model. Figure 1 shows the location of the smallest domains used in this paper to simulate each event.

3 Results

3.1 10 h accumulated precipitation

The three events have been selected due to their relatively large 10 h accumulated precipitation when comparing with other simulated events in the basin. Rain bands analyzed in other events over the Mediterranean basin (Mazon and Pino, 2009, 2013a, b) are associated with a lower amount of 10 h accumulated precipitation, between 0.1 and 10 mm, lasting from 1 to 5 h.

Figure 2 shows the simulated 10 h accumulated precipitation and the surface wind field at 10:00 UTC for (a) ISR, (b) GEN and (c) IP events. In the three cases, an offshore rain band is simulated near the coastline producing significant amount of precipitation when comparing with other simulated events in the Mediterranean basin.

The rain band observed in the ISR event was already studied by Mazon and Pino (2013b). However, the 10 h accumulated precipitation is shown in this paper for the first time. As described Mazon and Pino (2013b), this line of precipitation was quasi-stationary as a consequence of a strong drainage wind with similar wind speed to

NHESSD
1, 7595–7613, 2013

the prevailing synoptic wind. The 10 h accumulated precipitation reaches values higher than 24 mm in some parts of the rain band (see Fig. 2a).

The simulated rain band in the GEN event (see Fig. 2b) occurs due to a similar dynamics to the ISR rain band: a quasi-stationary line of convergence is simulated near the coastline, formed by interacting a similar synoptic prevailing flow with the cold inland drainage wind. In this case, the precipitation is lower than precipitation simulated for ISR, reaching the 10 h accumulated precipitation a maximum value near 14 mm.

The simulated rain band in the IP event is produced by a non-stationary coastal front, where a line of convergence moved offshore as the night progresses. Associated with this line of convergence, some precipitating cells are formed, producing more than 35 mm of 10 h accumulated precipitation in some parts of the rain band (see Fig. 2c).

3.2 1 h accumulated precipitation

Figure 3 shows 1 h accumulated precipitation and wind speed field at 00:00 and 06:00 UTC for the GEN event. During this event, an offshore line of convergence near the coastline that extends along 100 km and remains stationary during almost 6 h is simulated from 00:00 to 06:00 UTC (not shown). At 00:00 UTC (see Fig. 3a) several precipitation cells along the coastline are simulated at the boundary between the drainage and the prevailing synoptic flows. During the night, these cells moved onshore, but over the line of convergence new precipitation cells are continuously forming, as is shown in Fig. 3b. From 09:00 UTC, the rain bands dissipate because the wind speed of the cold air mass decreases.

Figure 4 shows 1 h accumulated precipitation and the surface wind field for the IP event at (a) 22:00 UTC on 5 September 2011, (b) at 03:00 and (b) 06:00 UTC on 6 September 2011. At 22:00 UTC on 5 September 2011, some small precipitation cells are simulated over the coastline. The convergence at sea–level between the cold air mass with a prevailing warmer easterly flow, acts as the triggering mechanism. As the cold air mass wind speed expands along the coastline, more precipitation cells are formed, while moving offshore. At 03:00 UTC (Fig. 4b) a rain band formed by several

NHESSD
1, 7595–7613, 2013

cells is simulated offshore, with around 100 km long. It is remarkable the large precipitation rate of the cells associated with this rain band, higher than 25 mm h^{-1}. The rain band moves offshore, and at 06:00 UTC (Fig. 4c) the simulation shows an arc of precipitation of around 150 km, formed by several intense convective cells. Behind the arc, the cold air mass flow turns from northwesterly to northeasterly, while ahead the arc a prevailing easterly flow exists. After sunrise, wind speed of the cold air mass decreases rapidly and at 10:00 UTC no precipitation cells are simulated (not shown).

3.3 Role of *H* in rain bands precipitation rate

The depth of the coastal front (H) plays an important role in enhancing convective precipitation, helping the warm and wet air mass to reach LFC. Coastal-front depth can be defined as the maximum height where a gradient of horizontal potential temperature exists. As an example, Fig. 5 shows at 03:00 UTC the vertical cross sections of potential temperature (color contour), equivalent potential temperature (closed lines), wind field (arrows) and liquid-water mixing-ratio (dashed lines) along the line AA′ indicated in Fig. 2 for the (a) GEN and (b) IP events. Following the criteria defined above, H takes values around 600–700 m in both events. The coastal-front depth for the ISR case is shown in Mazon and Pino (2013b), reaching around 800 m at 03:00 UTC and 1000 m at 06:00 UTC. In both Fig. 5a and b, the equivalent potential temperature decreases over the front, suggesting that weak instability exists. Consequently, the lifted relatively warm and wet air mass can reach LCL and LFC forming convective clouds higher than 1 km depth, as is shown the liquid-water mixing-ratio in Fig. 5a and b.

Assuming that a front acts as a mountain range blocking and lifting a prevailing warmer flow, the triggering parameter H/LFC is estimated for the three simulated nocturnal coastal fronts. Figure 6 shows the temporal evolution of H/LFC from 00:00 to 09:00 UTC for all the studied events. During the whole night H/LFC > 1, indicating that convective processes are occurring over the front. In all events, H decreases from 07:00 UTC and then the triggering parameter takes values lower than 1, indicating the end of convection. The triggering parameter estimated from other simulated coastal

NHESSD
1, 7595–7613, 2013

fronts over the Mediterranean basin (Mazon and Pino, 2013a, b), values lower than 1 are obtained during the whole night in those events associated with weak precipitation.

4 Conclusions

Three nocturnal coastal fronts formed near the coast by the interaction between a cold inland air mass that reaches the coast with a prevailing warmer and wetter air mass have been studied by using satellite observations, and WRF–ARW mesoscale model, contributing to the knowledge of this type of precipitation process in the Mediterranean basin.

According the simulations, nighttime rain bands are formed over an offshore line of convergence. Simulations show relatively large 1 and 10 h accumulated precipitation associated with these cells when comparing with some other simulated events over the Mediterranean basin. Due to similar values of the wind speed of the cold and warm air masses, the rain bands formed in the GEN and ISR events are quasi-stationary. The rain band occurred during IP event moves offshore.

Regardless the stationarity of the front, relatively large amount of 10 h accumulated precipitation are simulated, suggesting that some other factor associated with nocturnal coastal front has a larger contribution in producing heavy precipitation. Coastal-front depth (H) has been estimated and compared with LFC for the three events, evaluating the triggering parameter H/LFC (Miglietta and Rotunno, 2010). Assuming that the depth of nocturnal coastal front blocks and enhances vertical movements in a similar way that a mountain does, the evolution of the triggering parameter has been evaluated from 00:00 to 09:00 UTC. The triggering parameter takes values higher than 1 during almost the whole night, when rain bands are more developed, suggesting that the maritime warm and wet air mass is reaching the LFC. From around 07:00 UTC in all cases, H decreases and LFC remains almost constant for ISR and GEN events or increases for IP. Consequently, the triggering parameter decreases and takes values lower than 1. Summarizing, for the three simulated rain bands, if H/LFC is larger than

NHESSD
1, 7595–7613, 2013

1 rain bands are well developed, while values of the triggering parameter lower than 1 are observed when rain band are dissipating.

Acknowledgements. This project has been carried out by using the resources of the Supercomputing Center of Catalonia (CESCA) and it has been funded by the Spanish projects CGL2009-08609 and CGL2012-37416-C04-03.

References

Argueso, D., Hidalgo-Muñoz, J., Gamiz-Fortis, S., Esteban-Parra, M., Dudhia, J., and Castro-Diez, Y.: Evaluation of WRF parametrizations for climate studies over Southern Spain using a multistep regionalization, J. Climate, 24, 5633–5651, 2011. 7599

Callado, A. and Pascual, R.: Storms in front of the mouth rivers in north-eastern coast of Iberian peninsula, in: Proceedings, 4th Plinius Conference on Mediterranean Storms, Mallorca (Spain), available at: http://www.uib.es/depart/dfs/meteorologia/METEOROLOGIA/ROMU/informal/proceedings_4th_plinius_02/PDFs/Callado_and_Pascual.pdf, 2002. 7598

Dudhia, J.: Numerical study of convection observed during the winter monsoon experiment using a mesoscale two-dimensional model, J. Atmos. Sci., 46, 3077–3107, 1989. 7600

Frye, J. and Chen, Y.: Evolution of downslope flow under strong opposing trade winds and frequent trade-wind rainshowers over the island of Hawaii, Mon. Weather Rev., 129, 956–977, 2001. 7597

Goldreich, Y., Mozes, H., and Rosenfeld, D.: Radar analysis of cloud system and their rainfall yield in Israel, Israel J. Earth Sci., 53, 63–76, 2004. 7598

Grell, G. A., Dudhia, J., and Stauffer, D. R.: A description of the fifth generation Penn State/NCAR Mesoscale Model (MM5, Tech. Rep. TN–398+STR, NCAR, available at: http://nldr.library.ucar.edu/repository/assets/technotes/TECH-NOTE-000-000-000-214.pdf, 1994. 7598

Haddad, Z. S., Smith, E. A., Kummerow, C. D., Iguchi, T., Farrar, M. R., Durnen, S. L., Alves, M., and Olson, W. S.: The TRMM "day–1" radar/radiometer combined rain profiling algorithm, J. Meteorol. Soc. Jpn., 75, 799–809, 1997. 7599

Heiblum, R. H., Koren, I., and Altaratz, O.: Analyzing coastal precipitation using TRMM observations, Atmos. Chem. Phys., 11, 13201–13217, doi:10.5194/acp-11-13201-2011, 2011. 7598

NHESSD

1, 7595–7613, 2013

Hong, S.-H., Dudhia, J., and Chen, S.-H.: A revised approach to ice microphysical processes for the bulk parameterization of clouds and precipitation, Mon. Weather Rev., 132, 103–120, 2004. 7600
Hong, S.-Y. and Pan, H.-L.: Nonlocal boundary layer vertical diffusion in a medium-range forecast model, Mon. Weather Rev., 124, 2322–2339, 1996. 7600
Houze, R. A., Geostis, S. G., Marks, F. D., and West, A. K.: Winter monsoon convection in the vicinity of north Borneo, Part I: structure and time variation of the clouds and precipitation, Mon. Weather Rev., 109, 1595–1614, 1981. 7597
Huffman, G. J., Adler, R. F., Bolvin, D. T., Gu, G., Nelkin, E. J., Bowman, K. P., Hong, Y., Stocker, E. F., and Wolff, D. B.: The TRMM multi-satellite precipitation analysis: quasi-global, multi-year, combined-sensor precipitation estimates at fine scale, J. Hydrometeorol., 8, 38–55, 2007. 7599
Jankov, I., William, A., Moti, S., Shaw, B., and Koch, S.: The impact of different WRF model physical parametrization and their interaction on warm seasons MCS rainfall, Weather Forecast., 20, 1048–1060, 2005. 7599
Lau, J. and Yi-Leng, C.: A case study of nocturnal rain showers over windward coastal region of the island of Hawaii, Mon. Weather Rev., 127, 2674–2692, 1999. 7597
Laviola, S., Moscatello, A., Miglietta, M., Cattani, E., and Levizzani, V.: Satellite and numerical model investigation of two heavy events over central Mediterranan, J. Hydrometeorol., 12, 634–649, 2011. 7599
Mapes, B., Warner, T., Xu, M., and Negri, A.: Diurnal patterns of rainfall in northwestern South America, Part III: diurnal gravity waves and nocturnal convection offshore, Mon. Weather Rev., 131, 830–884, 2003. 7597
Mazon, J. and Pino, D.: Pluviometric anomaly in the Llobregat delta, J. Meteorol. Clim. Mediterr., 5, 31–50, 2009. 7598, 7600
Mazon, J. and Pino, D.: Nocturnal offshore precipitation near the Mediterranean coast of the Iberian Peninsula, Meteorol. Atmos. Phys., 120, 11–28, 2013a. 7598, 7600, 7603
Mazon, J. and Pino, D.: The role of sea–land air thermal difference, shape of the coastline, and sea surface temperature in the nocturnal offshore convection, Tellus A, 65, 20027, doi:10.3402/tellusa.v65i0.20027, 2013b. 7598, 7599, 7600, 7602, 7603
Miglietta, M. and Rotunno, R.: Numerical simulations of low-CAPE flows over a mountain ridge, J. Atmos. Sci., 67, 2391–2401, 2010. 7596, 7597, 7603

NHESSD
1, 7595–7613, 2013

Mlawer, E. J., Taubman, S.-J., Brown, P.-D., Iacono, M. J., and Clough, S. A.: Radiative transfer for inhomogeneous atmospheres: RRTM, a validated correlated-k model for the longwave, J. Geophys. Res., 102, 663–682, 1997. 7600

Mori, S., Hamada, J., Yamanaka, M., Okamoto, N., Murata, F., Sakurai, N., Hashiguchi, H., and Sribimawati, T.: Diurnal land–sea rainfall peak and migration over Sumatra island, Indonesian maritime continent observed by TRMM satellite and intensive rawinsonde soundings, Mon. Weather Rev., 132, 2021–2039, 2004. 7597

Murakami, M.: Analysis of the deep convective activity over the western Pacific and southeast Asia, J. Meteorol. Soc. Jpn., 61, 60–75, 1983. 7597

Neumann, J.: Land breezes and nocturnal thunderstorms, J. Meteorol., 8, 60–67, 1951. 7598

Ohsawa, T., Ueda, H., Hayashi, T., Watanabe, A., and Masumoto, J.: Diurnal variations of convective activity and rainfall in tropical Asia, J. Meteorol. Soc. Jpn., 79, 333–352, 2003. 7597

Ruiz, J. and Nogues-Paegle, J.: WRF model sensitivity to choice of parametrization over South America: validation against surface variables, Mon. Weather Rev., 138, 3342–3355, 2010. 7599

Schoenberg, L. M.: Doppler radar observation of land-breeze cold front, Geophys. Res. Lett., 112, 2455–2464, 1984. 7596

Skamarock, W. C., Klemp, J. B., Dudhia, J., Gill, D. O., Barker, D. M., Duda, M., Huang, X.-Y., and Powers, J. G.: A Description of the Advanced Research WRF Version 3, Tech. Rep. TN–475+STR, NCAR, 2008. 7597

Wapler, K. and Lane, T.: A case of offshore convective initiation by interacting land breezes near Darwin, Australia, Meteorol. Atmos. Phys., 5, 123–137, 2012. 7597

Wu, P., Yamanaka, M., and Matsumoto, J.: The formation of nocturnal rainfall offshore from convection over western Kalimantan (Borneo) island, J. Meteorol. Soc. Jpn., 86A, 187–203, 2008. 7597

Yu, C. and Jou, B.: Radar observations of the diurnal forced offshore convection lines among the southeastern coast of Taiwan, Mon. Weather Rev., 133, 1613–1636, 2004. 7597

NHESSD

1, 7595–7613, 2013

Table 1. Starting and run times, nested domains and location of the biggest domains used for each event in the WRF–ARW simulation.

Event	Date start (00:00 UTC)	Running time (h)	Horizontal domain resolution (km)	Center largest domain
ISR	4 Jan 2011	90	27, 9, 3, 1	32.1° N–34.8° E
GEN	28 Jan 2008	90	18, 6, 2	44° N–9° E
IP	6 Sep 2011	72	18, 6, 2	41.9° N–2.07° E

NHESSD
1, 7595–7613, 2013

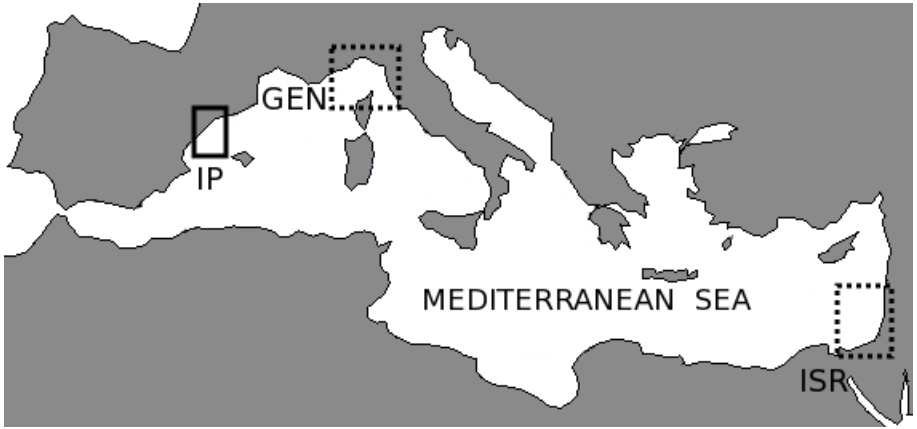

Fig. 1. Location of the nocturnal coastal fronts occurred on the Israel coast (ISR) on 6 January 2011, in the Gulf of Genoa (GEN) on 30 January 2008, and on the northeastern coast of the Iberian Peninsula (IP) on 6 September 2011. Squares approximately correspond to the smallest domains used in each of the WRF–ARW simulations. Dashed squares indicate quasi-stationary fronts, while close square indicates non stationary coastal front.

NHESSD
1, 7595–7613, 2013

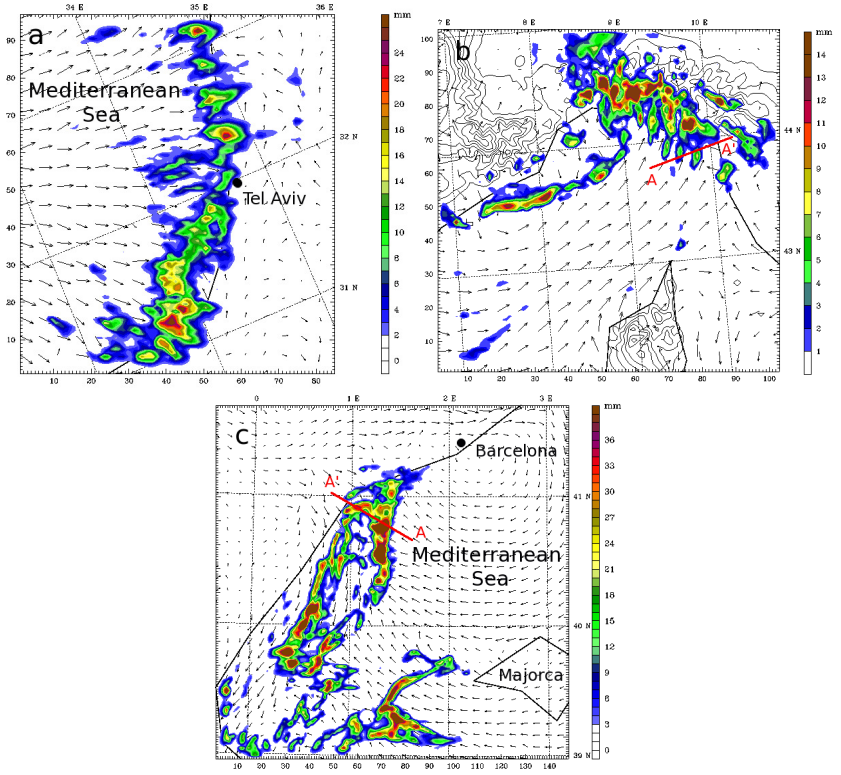

Fig. 2. 10 h accumulated precipitation (color contour) and surface wind field (arrows) at 10:00 UTC on **(a)** 6 January 2011 for ISR event (maximum wind vector 6.3 $m\,s^{-1}$), **(b)** on 30 January 2008 for GEN event (maximum wind vector 11 $m\,s^{-1}$), and **(c)** on 6 September 2011 for the IP event (maximum wind vector 9 $m\,s^{-1}$). The red line AA′ indicates the projection of the vertical cross section used to estimated the coastal-front depth. Note that the color scale for precipitation is not the same for the three panels.

NHESSD
1, 7595–7613, 2013

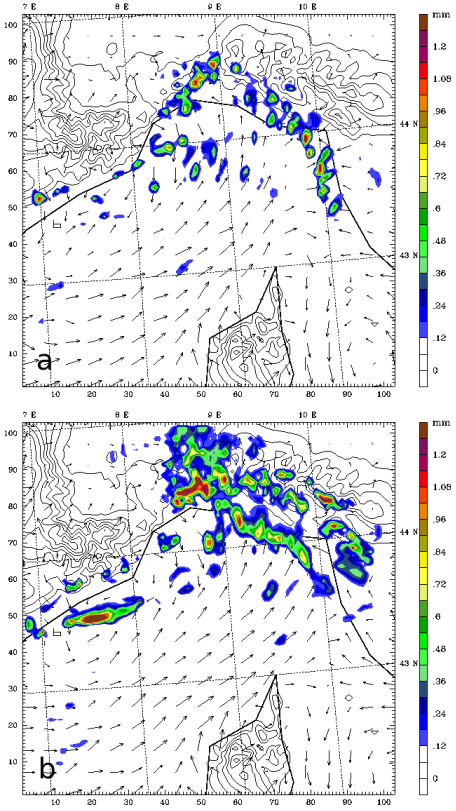

Fig. 3. 1 h accumulated precipitation (contour color) and surface wind field (arrows) at **(a)** 00:00 UTC (maximum wind vector 8.7 m s^{-1}) and **(b)** 06:00 UTC (maximum wind vector 9.7 m s^{-1}) on 30 January 2008 for the GEN event.

NHESSD
1, 7595–7613, 2013

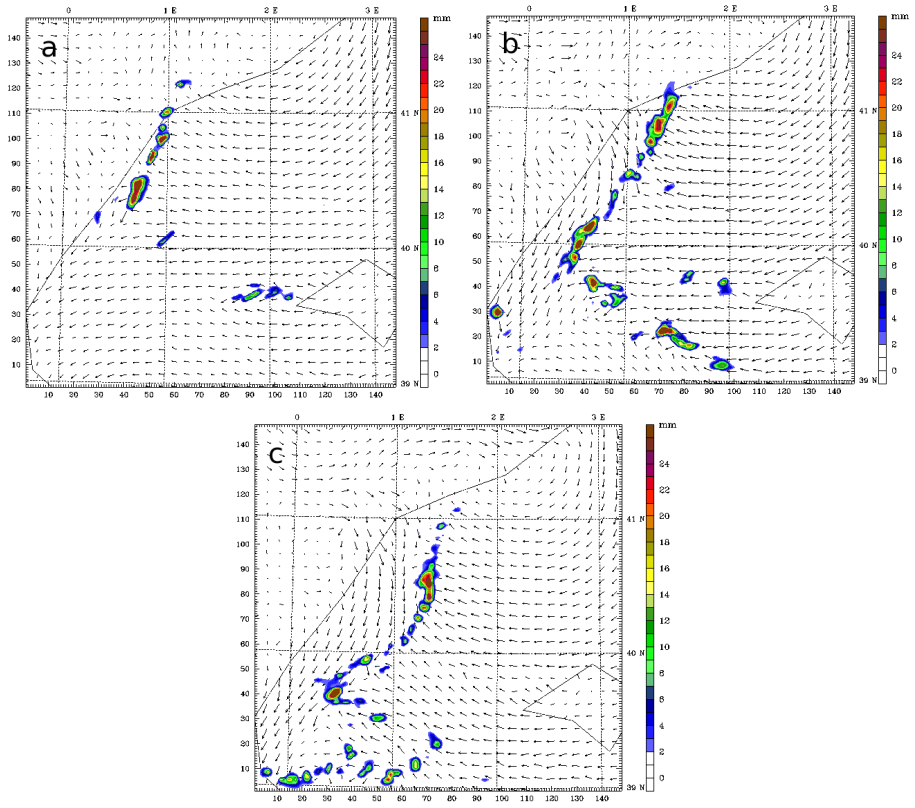

Fig. 4. 1 h accumulated precipitation (contour color) and surface wind field (arrows) at **(a)** 22:00 UTC (maximum wind vector 11.1 m s^{-1}) on 5 September 2011, **(b)** 03:00 UTC (maximum wind vector 9.8 m s^{-1}) and **(c)** 06:00 UTC (maximum wind vector 9 m s^{-1}) on 6 September 2011 for the IP event.

NHESSD
1, 7595–7613, 2013

Heavy nocturnal rain bands in the Mediterranean basin

J. Mazon and D. Pino

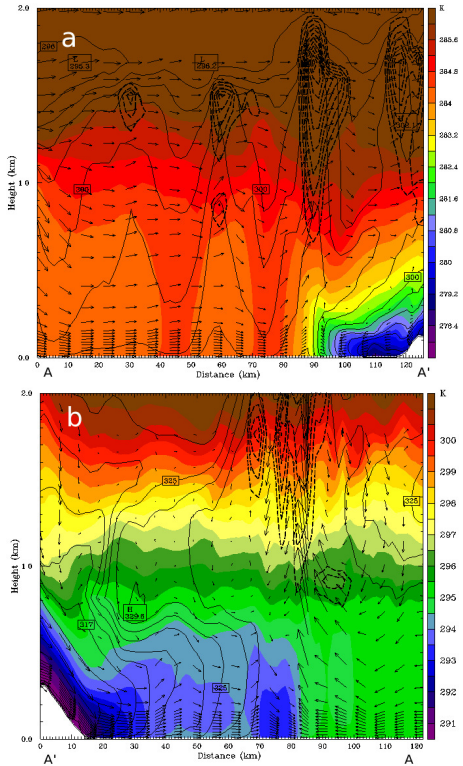

Fig. 5. Vertical cross section of the potential temperature (color contour), equivalent potential temperature (closed lines), liquid-water mixing-ratio (dashed lines) and wind field (arrows) along the red line AA′ defined in Fig. 2 at 03:00 UTC for the **(a)** GEN event (maximum horizontal wind vector 12.8 m s^{-1} and vertical 22.1 cm s^{-1}) and **(b)** IP event (maximum horizontal wind vector 10.2 m s^{-1}, vertical 58 cm s^{-1}).

NHESSD
1, 7595–7613, 2013

Heavy nocturnal rain bands in the Mediterranean basin

J. Mazon and D. Pino

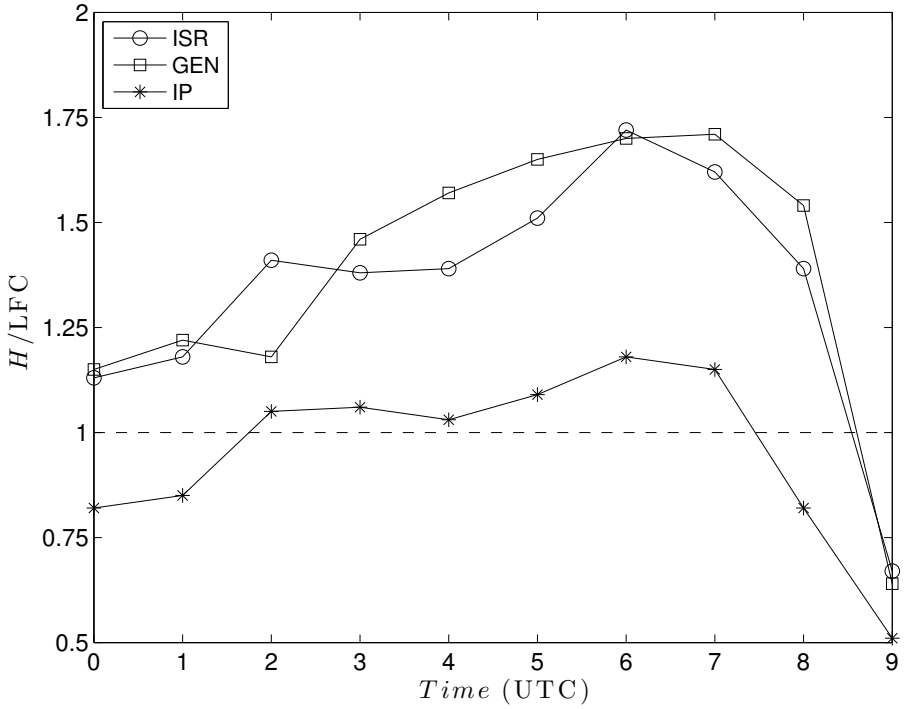

Fig. 6. Temporal evolution of the triggering parameter H/LFC from 00:00 to 09:00 UTC for the ISR event on 6 January 2011 (circles), GEN event on 30 January 2008 (squares) and IP event on 6 September 2011 (asterisks).

NHESSD
1, 7595–7613, 2013